J|A|C|S ARTICLES

Published on Web 08/03/2009

Solid-State NMR Investigations of the Immobilization of a BF_4^- Salt of a Palladium(II) Complex on Silica

Jerzy W. Wiench,[†] Christophe Michon,[†,#] Arkady Ellern,[‡] Paul Hazendonk,[§] Adriana Iuga,[§] Robert J. Angelici,[†,‡] and Marek Pruski*[,†,‡]

U.S. DOE Ames Laboratory, Iowa State University, Ames, Iowa 50011, Department of Chemistry, Iowa State University, Ames, Iowa 50011, and Department of Chemistry and Biochemistry, University of Lethbridge, Lethbridge, AB T1K 3M4, Canada

Received April 14, 2009; E-mail: mpruski@iastate.edu

Abstract: The structure of the silica supported palladium(II) complex $[Pd(dppp)(S_2C\text{-}NEt_2)]BF_4$ (abbreviated as $[Pd(dppp)(dtc)]BF_4$, where dppp is $Ph_2P(CH_2)_3PPh_2$) and interactions between the $[Pd(dppp)(dtc)]^+$ cation, the BF_4^- anion, and the silica surface are studied using solid-state NMR spectroscopy. The unsupported, crystalline form of $[Pd(dppp)(dtc)]BF_4$ is also investigated, both by X-ray diffraction and NMR. The structures of the cation and anion are found to be essentially the same in both unsupported and supported complex. The $[Pd(dppp)(dtc)]BF_4$ loading has been determined by quantitative measurements of ^{11}B, ^{19}F, and ^{31}P intensities, whereas the arrangement of anions and cations on the surface of silica has been established by two-dimensional heteronuclear correlation experiments involving ^1H, ^{11}B, ^{13}C, ^{19}F, ^{29}Si, and ^{31}P nuclei. At low coverages, the $[Pd(dppp)(dtc)]^+$ cations are located near the BF_4^- anions, which in turn are immobilized directly on the surface near the Q^4 sites. At higher loadings, which in this study corresponded to 0.06−0.15 mmol/g, the complexes stack on top of each other, despite the fact that the directly adsorbed molecules take up less than 10% of the silica surface. The relevance of these findings to heterogeneous catalysis is discussed.

1. Introduction

For the purpose of converting homogeneous transition metal complex catalysts into heterogeneous catalysts, a variety of metal complexes have been anchored on solid particles such as silica.[1−7] Often the homogeneous catalysts are attached to the solid through a covalent organic linker. On the other hand, there are a few examples of complexes that are anchored by hydrogen bonding through sulfonate($-SO_3^-$) groups in the complex to Si−OH groups on the silica surface.[8] An early report of this method describes the attachment of (sulfos)$Rh(CO)_2$ to silica through the $-SO_3^-$ group of the sulfos ligand, $^-O_3S-p-C_6H_4CH_2C(CH_2PPh_2)_3$, which is coordinated to the Rh through the three phosphine donor groups.[9] This heterogeneous catalyst was active in the hydroformylation of alkenes. A complex $[(R,R\text{−Me-DuPHOS})Rh(COD)]CF_3SO_3$, in which the $-SO_3^-$ group is part of the $CF_3SO_3^-$ anion, adsorbs to silica by hydrogen bonding. This solid catalyzes the enantioselective hydrogenation of prochiral olefins.[10]

In previous studies,[11] we investigated the adsorption of $(\eta^5\text{-}C_5H_5)Ru(CO)_2(BF_4)$ on mesoporous silica (SBA-15). It was observed that the ν(SiO-H) band at 3742 cm^{-1} in SBA-15 essentially disappears when $(\eta^5\text{-}C_5H_5)Ru(CO)_2(BF_4)$ is adsorbed onto the SBA-15, which suggests that BF_4^- is hydrogen-bonding to surface Si−OH groups. This $(\eta^5\text{-}C_5H_5)Ru(CO)_2(BF_4)$/SBA-15 solid was used to extract dibenzothiophenes from model petroleum feedstocks.[11] Support for the proposal that BF_4^- hydrogen-bonding anchors the $(\eta^5\text{-}C_5H_5)Ru(CO)_2(BF_4)$ complex onto the silica was provided by an IR study of $[(n\text{-}Bu)_4N]BF_4$ adsorbed on SBA-15, which also showed the absence of the ν(SiO−H) band. Since it is unlikely that $[(n\text{-}Bu)_4N]^+$ cations are able to bond to Si−OH groups, it is probably the BF_4^- anions that are hydrogen-bonding to the Si−OH groups. This conclusion suggests that other BF_4^- salts, including those of cationic metal complex catalysts, could be anchored onto silica. The BF_4^- anion with such cationic complexes has the advantage over

[†] Ames Laboratory, Iowa State University.
[#] Current address: Université de Sciences et Technologies de Lille UCCS - UMR8181 CNRS - SOMC team - ENSCL BP90108, 59652 Villeneuve d'Ascq, France.
[‡] Department of Chemistry, Iowa State University.
[§] Department of Chemistry and Biochemistry, University of Lethbridge.

(1) Bluemel, J. *Coord. Chem. Rev.* **2008**, *252*, 2410–2423.
(2) Anwander, R. In *Handbook of Heterogeneous Catalysis*; 2nd ed.; Ertl, G., Ed.; Wiley-VCH Verlag: Weinheim, 2008; p 583−614.
(3) El-Nahhal, I. M.; El-Ashgar, N. M. *J. Organomet. Chem.* **2007**, *692*, 2861–2886.
(4) Vos, D. E.; Vankelecom, I. F. J.; Jacobs, P. A. *Chiral Catalyst Immobilization and Recycling*; Wiley-VCH: New York, 2000.
(5) Valkenberg, M. H.; Holderich, W. F. *Catal. Rev. - Sci. Eng.* **2002**, *44*, 321–374.
(6) Gladysz, J. A. *Chem. Rev.* **2002**, *102*, 3215–3216.
(7) Toth, I.; Van Geem, P. In *Encyclopedia of Catalysis*; Horvath, I. T., Ed.; Wiley & Sons: New York, 2003; Vol. 4, p 164.
(8) Fraile, J. M.; Garcia, J. I.; Mayoral, J. A. *Chem. Rev.* **2009**, *109*, 360–417.
(9) Bianchini, C.; Burnaby, D. G.; Evans, J.; Frediani, P.; Meli, A.; Oberhauser, W.; Psaro, R.; Sordelli, L.; Vizza, F. *J. Am. Chem. Soc.* **1999**, *121*, 5961–5971.
(10) de Rege, F. M.; Morita, D. K.; Ott, K. C.; Tumas, W.; Broene, R. D. *Chem. Commun.* **2000**, 1797–1798.
(11) McKinley, S. G.; Vecchi, P. A.; Ellern, A.; Angelici, R. J. *Dalton Trans.* **2004**, 788–793.

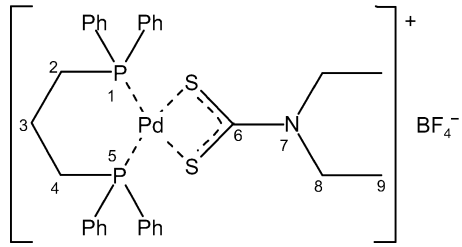

Figure 1. The $[Pd(dppp)(dtc)]BF_4$ complex.

sulfonate salts that it is less strongly coordinating to the metal, thereby allowing the metal center to be more active as a catalyst.

Solid-state NMR is one of the key techniques to investigate the structure of inorganic mesoporous solids.[12−16] An earlier study[17] of the adsorption of the BF_4^- salt $[Rh_2(NCCH_3)_{10}](BF_4)_4$ on the mesoporous silica MCM-41 by ^{11}B, ^{13}C, and ^{29}Si MAS NMR, as well as FTIR, Raman, and EXAFS spectroscopy, suggested that the compound was attached to the MCM-41 surface through Si−O−Rh bonds. An investigation[18] of the attachment of $[(\eta^5\text{-}C_5H_5)Fe(CO)_2(THF)]BF_4$ to amorphous silica gel led to the conclusion that the BF_4^- anion reacted with the silica surface to give Si−O−BF_3^- and Si−O−BF_2 linkages.

The goal of the present study was to investigate in detail the nature of the interactions between the surface of amorphous silica and the cation and BF_4^- anion of $[Pd(dppp)(dtc)]BF_4$ (Figure 1), where dppp is 1,3-bis(diphenylphosphino)propane and dtc is *N*,*N*-diethyldithiocarbamate. We chose the $[Pd(dpp)(dtc)]^+$ complex because it is air-stable and contains NMR-active ^{31}P atoms. The presence of NMR-active nuclei in both the cation and anion in $[Pd(dppp)(dtc)]BF_4$ offers the possibility of probing the relative positions of these ions on the silica surface. The structure of the supported $[Pd(dppp)(dtc)]BF_4$ complex and the nature of its attachment to the silica surface are detailed using several one- and two-dimensional (1D and 2D) solid-state NMR experiments involving ^1H, ^{11}B, ^{13}C, ^{19}F, ^{29}Si, and ^{31}P nuclei. Unexpectedly, we found that at loadings exceeding ~0.04 mmol/g, the complexes stack on top of each other, even though the directly adsorbed molecules take up less than 10% of the silica surface.

2. Experimental Section

2.1. Sample Preparations. 2.1.1. (*N*,*N*-Diethyldithiocarbamato)[1,3-bis(diphenylphosphino)propane]palladium(II) Tetrafluoroborate, $[Pd(dppp)(dtc)]BF_4$. Dichloro[1,3-bis(diphenylphosphino)propane]palladium[19,20] (0.68 g, 1.15 mmol), sodium *N*,*N*-diethyldithiocarbamate (0.26 g, 1.15 mmol), and silver tetrafluoroborate (0.23 g, 1.15 mmol) were heated under reflux in 100 mL of acetonitrile (dried over CaH_2) for 3 h under an argon atmosphere. The resulting solution was cooled at room temperature and then filtered through a plug of dry Celite under argon; the residue was washed with dichloromethane (20 mL). The resulting solution was evaporated to dryness to give a pale yellow solid, which was washed with dry diethylether and recrystallized two times with dry dichloromethane and *n*-hexane (yield 90%, 0.78 g, 1.04 mmol). Elem. Anal. Calcd for $C_{32}H_{36}P_2S_2NPdBF_4$ with 1/3 molecule of CH_2Cl_2: C, 49.65%; H, 4.69%; N, 1.79%; S, 8.21%. Found: C, 49.75%; H, 4.98%; N, 2.20%; S, 8.17%. IR (CH_2Cl_2) ν (cm^{-1}): 1522s (ν C−N), 1101s, 1060s (ν C−S). Atom labels for NMR assignments are shown in Figure 1. ^1H NMR 400.1 MHz ($CDCl_3$) δ (ppm): 7.48 (m, 8H, H*m*), 7.43 (m, 4H, H*p*), 7.38 (m, 8H, H*o*), 3.61 (q, 4H, H8, $^3J = 7.2$ Hz), 2.79 (m, 4H, H2 and H4), 2.20 (m, 2H, H3), 1.17 (t, 6H, H9, $^3J = 7.2$ Hz). ^{31}P NMR 161.9 MHz ($CDCl_3$) δ (ppm): 10.57 (s, P1 and P5). ^{13}C NMR 100.6 MHz ($CDCl_3$) δ (ppm): 204.3 (1C, C6), 132.8 (t, 8C, C*o*, $^{P-Co}J = 5.5$ Hz), 131.7 (s, 4C, C*p*), 129.1 (t, 8C, C*m*, $^{P-Cm}J = 5.5$ Hz), 128.0 (q, 4C, C*i*, $^{P-Ci}J = 24.4$ and 1.3 Hz), 44.2 (2C, C8), 23.6 (2C, C2 and C4, $^{P-C}J = 18.2$ Hz), 18.6 (1C, C3), 12.4 (2C, C9).

2.1.2. D_2O Exchanged SiO_2. Silica gel (Aldrich, 200−400 mesh, 60 Å pores, 500 m^2/g BET surface area, 0.75 cm^3/g pore volume) was dried 12 h under dynamic vacuum at 100 °C. To reduce the unwanted ^1H NMR background, to this silica was added D_2O (10 mL/g of silica) and the mixture was stirred for 5 min. The liquids were removed by pipet and the resulting silica was dried under dynamic vacuum 12 h at 100 °C. During our earlier studies of mesoporous silica,[16] we have used quantitative ^1H MAS NMR to determine that approximately 90% of the OH groups are converted to OD under such conditions. This D_2O-treated silica was used for the preparation of the supported tetrafluoroborate salts.

2.1.3. General Procedure for the Preparation of Supported $[Pd(dppp)(dtc)]BF_4$ on Silica. The desired amount of the complex was dissolved in 10 mL of dichloromethane (dried on alumina using a Solv-Tek solvent purification system). The resulting solution was transferred to the Schlenk flask containing 0.5 g of D_2O-treated silica under an argon atmosphere. This mixture was stirred for 1 h. After evaporation of the solvent under dynamic vacuum, the remaining solid was dried for 12 h at 100 °C under 10^{-5} Torr. Three samples were prepared with the intended concentrations of 0.048, 0.095, and 0.19 mmol of the Pd(II) complex per gram of silica. To minimize rehydration of the surface, the silica and supported $[Pd(dppp)(dtc)]BF_4$ samples were stored in a desiccator under nitrogen. By using quantitative ^{11}B, ^{19}F, and ^{31}P NMR spectra, we have determined that the concentrations were 0.06, 0.12, and 0.15 mmol/g (see section 3.2.2); these samples are labeled PdBS06, PdBS12 and PdBS15, respectively.

2.2. NMR Measurements. Liquid-state NMR spectra of the palladium complex were measured on Bruker DRX 400 MHz (9.4 T) spectrometer in 5 mm glass tubes. 1D and 2D solid-state NMR data were acquired on Chemagnetics Infinity 400, Varian INOVA 500 and Varian NMR System 600 spectrometers equipped with 9.4, 11.7, and 14.1 T magnets, respectively. At 9.4 T, the spectra were acquired at 400.1 (^1H), 376.3 (^{19}F), 161.9 (^{31}P), 128.3 (^{11}B), 100.7 (^{13}C), and 79.4 (^{29}Si) MHz, using a 1.7-mm double tuned probe (A. Samoson[21]) with a maximum magic angle spinning (MAS) rate of 40 kHz. This probe did not produce any background signals that could interfere with our measurements. The INOVA 500 spectrometer used 500.0 MHz for ^1H, 470.4 MHz for ^{19}F, 125.6 MHz for ^{13}C, and a 4.0 mm quadruple resonance HFXY probe. The 14.1 T system, which operated at 599.7, 564.2, 242.7, 150.8, and 119.4 MHz for ^1H, ^{19}F, ^{31}P, ^{13}C, and ^{29}Si nuclei, used a 3.2-mm Varian triple tuned probe capable of MAS at 25 kHz. All

(12) Epping, J. D.; Chmelka, B. F. *Curr. Opin. Colloid Interface Sci.* **2006**, *11*, 81–117.
(13) Bonhomme, C.; Coelho, C.; Baccile, N.; Gervais, C.; Azais, T.; Babonneau, F. *Acc. Chem. Res.* **2007**, *40*, 738–746.
(14) Buntkowsky, G.; Breitzke, H.; Adamczyk, A.; Roelofs, F.; Emmler, T.; Gedat, E.; Gruenberg, B.; Xu, Y.; Limbach, H.-H.; Shenderovich, I.; Vyalikh, A.; Findenegg, G. *Phys. Chem. Chem. Phys.* **2007**, *9*, 4843–4853.
(15) Trebosc, J.; Wiench, J. W.; Huh, S.; Lin, V. S. Y.; Pruski, M. *J. Am. Chem. Soc.* **2005**, *127*, 3057–3068.
(16) Trebosc, J.; Wiench, J. W.; Huh, S.; Lin, V. S. Y.; Pruski, M. *J. Am. Chem. Soc.* **2005**, *127*, 7587–7593.
(17) Pillinger, M.; Nunes, C. D.; Vaz, P. D.; Valente, A. A.; Goncalves, I. S.; Ribeiro-Claro, P. J. A.; Rocha, J.; Carlos, L. D.; Kuehn, F. E. *Phys. Chem. Chem. Phys.* **2002**, *4*, 3098–3105.
(18) Casper, D. J.; Sklyarov, A. V.; Hardcastle, S.; Barr, T. L.; Foersterling, F. H.; Surerus, K. F.; Hossain, M. M. *Inorg. Chim. Acta* **2006**, *359*, 3129–3138.
(19) Exarchos, G.; Robinson, S. D.; Steed, J. W. *Polyhedron* **2000**, *19*, 1511–1517.
(20) Exarchos, G.; Nyburg, S. C.; Robinson, S. D. *Polyhedron* **1998**, *17*, 1257–1266.
(21) Samoson, A.; Tuherm, T.; Past, J.; Reinhold, A.; Anupold, T.; Heinmaa, I. *Top. Curr. Chem.* **2005**, *246*, 15–31.

spectra were acquired under MAS using direct polarization (DPMAS) or cross-polarization (CPMAS). The $^{13}C\{^{19}F\}$, $^{19}F\{^{11}B\}$, and $^{31}P\{^{1}H\}$ spectra were only acquired in one dimension. The 2D measurements included homonuclear $^{19}F-^{19}F$ methods (RFDR and double-quantum (DQMAS)) and heteronuclear correlation (HETCOR) experiments with the following pairs of nuclei: $^{11}B\{^{1}H\}$, $^{13}C\{^{1}H\}$, $^{19}F\{^{1}H\}$, $^{29}Si\{^{1}H\}$, $^{29}Si\{^{19}F\}$, and $^{31}P\{^{19}F\}$. The DQ coherences were created and converted to single quantum (SQ) coherences using back-to-back (BABA) pulse sequence[22] under 40 kHz MAS. The CP and HETCOR spectra used dipolar cross-polarization with the radiofrequency (RF) magnetic field ramped in the {X} channel around the first sideband of the Hartmann−Hahn matching curve. With the exception of the 2D $^{13}C\{^{1}H\}$ and $^{19}F\{^{1}H\}$ HETCOR spectra, ^{1}H or ^{19}F homonuclear decoupling relied on fast MAS at 40 kHz.[15,16] The $^{13}C\{^{1}H\}$ spectra of the bulk [Pd(dppp)-(dtc)]BF_4 and sample PdBS15 were obtained under 8 kHz MAS, using ^{1}H homonuclear decoupling via the frequency-switched Lee-Goldburg (FSLG[23]) method and total sideband suppression (TOSS[24]). Homonuclear ^{1}H decoupling during the evolution period of $^{19}F\{^{1}H\}$ experiments was obtained using the phase-modulated Lee-Goldburg (PMLG)[25] method. Heteronuclear ^{1}H (and/or ^{19}F) decoupling was obtained under high power continuous wave RF irradiation or via TPPM.[26] The sensitivity of measurements involving ^{29}Si detection was significantly increased by using a Carr−Purcell−Meiboom−Gill (CPMG) sequence of π pulses to refocus the silicon magnetization.[27,28]

The spin counting measurements of ^{19}F, ^{11}B, and ^{31}P were performed under 40 kHz MAS using single pulse DPMAS and relaxation delay $\geq 5T_1$. The intensities measured in silica supported samples were compared with the corresponding signal obtained for the bulk complex.

All NMR measurements were performed at room temperature. The samples were transferred to the MAS rotors under a dry nitrogen atmosphere. Prior to the HETCOR experiments involving ^{1}H nuclei, with the exception of the $^{19}F\{^{1}H\}$ measurement, the samples were also evacuated at room temperature for 2 h to eliminate any potential influence of rehydration on the spectra. The heating due to friction between the rotor and the air, which may have increased the sample temperature by up to 15 °C above the ambient under 40 kHz MAS,[15,29] was not compensated. The values of other key experimental parameters used in the NMR measurements are given in the figure captions, where B_0 denotes the external magnetic field, ν_R the sample rotation rate, ν_{RF}^X the magnitude of radiofrequency magnetic field applied to X spins, τ_{CP} the cross-polarization time, N_{CPMG} the number of echoes acquired in CPMG experiments, τ_{CPMG} the corresponding time interval between π pulses, τ_{RD} the relaxation delay, and NS the number of scans. In the case of 2D spectra, only the total acquisition time AT is given for the sake of simplicity. The 1D projections of 2D spectra are plotted using the skyline mode. The chemical shifts are reported using the δ scale and are referenced to TMS (^{1}H, ^{13}C and ^{29}Si), Et_2OBF_3 (^{11}B), $CFCl_3$ (^{19}F), and 85% H_3PO_4 (^{31}P), all at 0 ppm.

2.3. XRD Measurements. For X-ray measurements, the [Pd-(dppp)(dtc)]BF_4 sample was crystallized from chloroform. A colorless crystal with approximate dimensions 0.4 × 0.27 × 0.20 mm^3 was selected under ambient conditions. The crystal was mounted and centered in the X-ray beam using a video camera.

Table 1. Acquisition and Refinement Data for the X-ray Diffraction Analysis of [Pd(dppp)(dtc)]$BF_4 \cdot 2CHCl_3$[a]

formula	$C_{32}H_{36}NP_2PdS_2BF_4 \cdot 2\ CHCl_3$
mol wt	992.62
cryst syst	Monoclinic
space group	$P2_1/n$
a (Å)	15.817(3)
b (Å)	17.210(3)
c (Å)	15.875(3)
α (deg)	90
β (deg)	94.079(3)
γ (deg)	90
V (Å^3)	4310.4(13)
Z	4
color	Colorless
cryst dimens (mm)	0.4 × 0.27 × 0.20
D_{calcd} (g cm^{-3})	1.53
F_{000}	2000
μ (mm^{-1})	1.017
temp. (K)	183(2)
Index ranges	$-20 \leq h \leq 20$, $-22 \leq k \leq 22$, $-21 \leq l \leq 21$
θ limits (deg)	1.75/28.29
Reflections collected	39306
Observed reflections [R(int)]	10288 [R(int) = 0.0299]
Final R_1, $wR_2[I > 2\sigma(I)]$	0.0442, 0.1174
R_1, wR_2 (all data)	0.0579, 0.1305
GOF	1.044
Largest peak in final diff map and hole (eÅ^{-3})	1.563 and −0.930

[a] All measurements were performed with a Bruker CCD-1000 diffractometer using Mo Kα graphite monochromated radiation (Wavelength, 0.71073 (Å); Scan Mode, 'phi scans'). $R_1 = \sum ||Fo| - |F_c||/\sum |F_o|$ and $wR_2 = \{\sum[\ w(F_o^2 - F_c^2)^2\ ]/\sum\ [w(F_o^2)^2]\}^{1/2}$.

The crystal evaluation and data collection were performed at 183 K on a Bruker CCD-1000 diffractometer with Mo Kα ($\lambda = 0.71073$ Å) radiation and the detector to crystal distance of 5.03 cm. The initial cell constants were obtained from three series of ω scans at different starting angles. Each series consisted of 30 frames collected at intervals of 0.3° in a 10° range about ω with an exposure time of 5 s per frame. A total of 137 reflections were obtained. The reflections were successfully indexed by an automated indexing routine in the SMART program. The final cell constants were calculated from a set of 1021 strong reflections from the actual data collection. The data were collected using the full sphere routine. A total of 39 306 data were harvested by collecting four sets of frames with 0.3° scans in ω with an exposure time of 5 s per frame. This data set was corrected for Lorentz and polarization effects. The absorption correction was based on fitting a function to the empirical transmission surface as sampled by multiple equivalent measurements[30] using SADABS software.[31]

The [Pd(dppp)(dtc)]BF_4 complex crystallized with two $CHCl_3$ molecules as monoclinic crystallites, in space group $P2_1/n$. The unit cell data and refinement parameters are presented in Table 1, whereas atomic coordinates, bond lengths and angles, and atomic displacement information are available in the Supporting Information.[32] The positions of heavy atoms were found by the Patterson method, while the remaining atoms were located in an alternating series of least-squares cycles and difference Fourier maps. All non-hydrogen atoms were refined in a full-matrix anisotropic approximation including counterion and two $CHCl_3$ solvent molecules per complex. All hydrogen atoms were placed in the structure factor calculation at idealized positions and were allowed to ride on the neighboring atoms with relative isotropic displacement coefficients.

(22) Feike, M.; Demco, D. E.; Graf, R.; Gottwald, J.; Hafner, S.; Spiess, H. W. *J. Magn. Reson. A* **1996**, *122*, 214–221.
(23) Bielecki, A.; Kolbert, A. C.; De Groot, H. J. M.; Griffin, R. G.; Levitt, M. H. *Adv. Magn. Reson.* **1990**, *14*, 111.
(24) Dixon, W. T. *J. Chem. Phys.* **1982**, *77*, 1800–1808.
(25) Vinogradov, E.; Madhu, P. K.; Vega, S. *Chem. Phys. Lett.* **1999**, *314*, 443–450.
(26) Bennett, A. E.; Rienstra, C. M.; Auger, M.; Lakshmi, K. V.; Griffin, R. G. *J. Chem. Phys.* **1995**, *103*, 6951–6958.
(27) Meiboom, S.; Gill, D. *Rev. Sci. Instrum.* **1958**, *29*, 688–691.
(28) Wiench, J. W.; Lin, V. S. Y.; Pruski, M. *J. Magn. Reson.* **2008**, *193*, 233–242.
(29) Bielecki, A.; Burum, D. P. *J. Magn. Reson. A* **1995**, *116*, 215–220.
(30) Blessing, R. H. *Acta Crystallogr., Sect. A* **1995**, *A51*, 33–38.
(31) All software and sources of the scattering factors are contained in the SHELXTL (version 5.1) program library (G. Sheldrick, Bruker Analytical X-Ray Systems, Madison, WI).
(32) See Supporting Information.

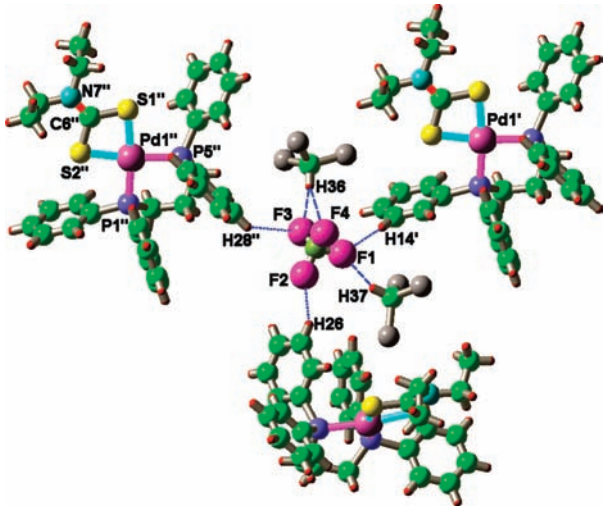

Figure 2. 'Ball and stick' structure of $[Pd(dppp)(dtc)]BF_4$ complex[32] with two $CHCl_3$ molecules and two neighboring $[Pd(dppp)(dtc)]$ cations. Short (<2.7 Å) and long (>3.2 Å) hydrogen bonds to fluorine atoms are shown as blue dashed and dotted lines, respectively. Other bonds: Pd−P (magenta), Pd−S (turquoise), and N7−C6 (red) are also marked.

Final least-squares refinement of 462 parameters against 10 288 independent reflections converged to R (based on F^2 for $I \geq 2\sigma$) and wR (based on F^2 for $I \geq 2\sigma$) of 0.044 and 0.118, respectively. The ORTEP structure shown in the Supporting Information was drawn at the 50% probability level. The resulting CIF file has been tested with PLATON software.[33]

2.4. Other Characterization Methods. IR spectra were measured with a Nicolet Magna 560 spectrometer. Elemental analyses were performed on a Perkin-Elmer 2400 Series II CHNS/O analyzer at the Iowa State University Chemistry Department.

3. Results and Discussion

3.1. XRD Study of the Crystalline $[Pd(dppp)(dtc)]BF_4$ Complex. The structure of $[Pd(dppp)(dtc)]BF_4 \cdot 2CHCl_3$. (Figure 2), as determined by single-crystal X-ray diffraction,[32] shows that the $[Pd(dppp)(dtc)]^+$ cation is square planar around the Pd with Pd−S (2.3400(9), 2.3536(9) Å) and Pd−P distances (2.2699(9), 2.2679(9) Å) that are the same within experimental error as those in the same cation in $[Pd(dppp)(dtc)]_2HgCl_4 \cdot CH_2Cl_2 \cdot H_2O$.[19] The S1−Pd−S2 (75.54(3)°) and P1−Pd−P5 angles (90.72(4)°) are essentially the same as those in the $HgCl_4^{2-}$ compound. The short N7−C6 bond distance (1.318 Å) is characteristic of other dtc complexes and indicates N → C π bonding.[19,20] The BF_4^- anion is distorted from tetrahedral geometry as indicated by the F−B−F angles which range from 96.2 to 119.9°. This distortion is likely due to a network of hydrogen bonds between the BF_4^- fluorine atoms and the $CHCl_3$ molecules or the phenyl groups of the dppp ligands. The shortest F···H distances are with the C−H protons of the $CHCl_3$ molecules: 2.185 (F3···H36) and 2.204 Å (F1···H37). There is also a short F1···H(14′) distance (2.514 Å) to a C−H proton in the meta position of a phenyl ring and a slightly longer F4···H36 distance of 2.649 Å to a $CHCl_3$ molecule. Other F···H distances are longer, including those between BF_4^- fluorine atoms and meta protons in phenyl groups, which are 3.2 Å or larger (Figure 2). Hydrogen bonding between fluorine atoms in BF_4^- anions and C−H protons in a variety of organometallic cations and solvent molecules have been observed previously.[34,35] In $[Pd(dppp)(dtc)]_2HgCl_4 \cdot CH_2Cl_2 \cdot H_2O$,[19] a related network of hydrogen bonds was also observed between chlorine atoms of the $HgCl_4^{2-}$ anion and phenyl C−H hydrogen atoms of the dppp ligand and hydrogen atoms of the solvent molecules.

3.2. NMR Characterization of the Crystalline and Silica-Supported $[Pd(dppp)(dtc)]BF_4$ Complex. We used a suite of 2D correlation methods to examine the structure of the supported complex and to delineate the location of its cationic and anionic parts on the silica surface. To simplify the discussion, we first present and compare the results obtained for the $[Pd(dppp)(dtc)]^+$ cation and BF_4^- anion in the bulk (crystalline) and supported samples (sections 3.2.1 and 3.2.2, respectively). The interactions between the cationic and anionic parts of the complex in both environments are investigated in section 3.2.3, which is followed by the discussion of the interactions between the BF_4^- and the surface and the cationic complex and the surface, in sections 3.2.4 and 3.2.5, respectively. Finally, in the Conclusion, we summarize our results and propose a model for the anchoring of $[Pd(dppp)(dtc)]BF_4$ on the silica surface, and discuss the relevance of our findings to catalysis.

3.2.1. NMR Spectra of the Crystalline $[Pd(dppp)(dtc)]BF_4$ Complex. The NMR spectra of the unsupported complex were measured both in solution (^{13}C and ^{31}P, see Figure 3a,b) and in solid state (^{13}C, ^{31}P, ^{19}F, and ^{11}B, see Figure 3c−g). The ^{13}C and ^{31}P chemical shifts (Table 2) obtained in $CDCl_3$ solution are similar to those reported for other dithiocarbamatodiphosphine palladium(II) complexes.[19,20,36] Because of fast molecular motion of the hexagonal rings, phosphorus sites P1 and P5 are magnetically equivalent and thus appear as a single resonance in Figure 3b. Also equivalent are carbons C2 and C4 in diphosphinopropane ring, as well as those in positions *ipso*, *ortho*, *meta*, and *para* in all four phenyl rings (see Table 2 and Figure 3a).

In the $^{31}P\{^1H\}$ CPMAS spectrum of the solid phase, two phosphorus resonances are observed (Figure 3d), which confirms the lack of symmetry in the diphosphinopropane ring found by XRD.[32] Similarly, the solid-state ^{13}C NMR spectra exhibit more resonances than has been found in solution. This is evident in the 1D $^{13}C\{^1H\}$ CPMAS spectrum of Figure 3c, which is very convoluted in the aromatic region. In the 2D $^{13}C\{^1H\}$ HETCOR spectrum, the ^{13}C resonances are separated along the ^1H dimension (Figure 3g). More than 20 resonances attributable to carbons in the phenyl rings were identified, whose chemical shifts are listed at the bottom of Table 2. As will be shown below, the resonances at around 130 ppm are indistinguishable in the silica supported $[Pd(dppp)(dtc)]BF_4$ complex (due to heterogeneity of the local environments); thus, no attempt was made to assign resonances in this spectral range to specific sites. As expected, the peak due to chloroform, which is prominent in the solution spectrum at 77 ppm, is lacking in the solid-state spectra.

The ^{19}F and ^{11}B DPMAS spectra of Figure 3e,f exhibit a single resonance corresponding to the BF_4^- anion. The ^{19}F and

(33) Spek, A. L. *J. Appl. Crystallogr.* **2003**, *36*, 7–13.
(34) Braga, D.; Maini, L.; Polito, M.; Grepioni, F. *Struct. Bonding (Berlin, Ger.)* **2004**, *111*, 1–32.
(35) Braga, D.; Grepioni, F. *NATO Sci. Ser., Ser. C* **1999**, *519*, 173–191.
(36) Yih, K.-H.; Lee, G.-H.; Wang, Y. *J. Chin. Chem. Soc.* **2004**, *51*, 31–36.
(37) Wray, V. In *Annual Reports on NMR Spectroscopy*; Webb, G. A., Ed.; Academic Press: London, 1980; Vol. 10a, p 3−508.
(38) Fochi, F.; Jacopozzi, P.; Wegelius, E.; Rissanen, K.; Cozzini, P.; Marastoni, E.; Fisicaro, E.; Manini, P.; Fokkens, R.; Dalcanale, E. *J. Am. Chem. Soc.* **2001**, *123*, 7539–7552.
(39) Bondarev, O. G.; Mikhel, I. S.; Tsarev, V. N.; Petrovskii, P. V.; Davankov, V. A.; Gavrilov, K. N. *Russ. Chem. Bull.* **2003**, *52*, 116–121.

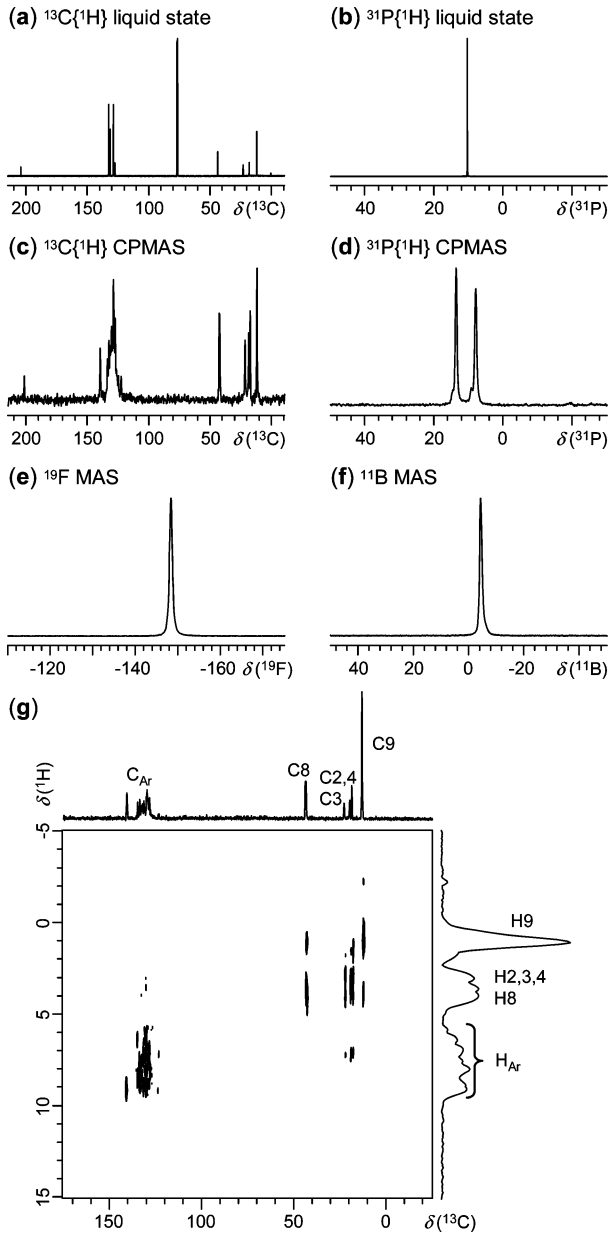

Figure 3. (a−f) 1D NMR spectra of [Pd(dppp)(dtc)]BF$_4$ in solution (a and b) and in solid state (c−f). (g) ^{13}C{^{1}H} FSLG-HETCOR spectrum of solid [Pd(dppp)(dtc)]BF$_4$. Experimental conditions: B_0 = 9.4 T (a, b, e, f) and 14.1 T (c, d, g); ν_R = 8 kHz (c, d, g) and 40 kHz (e, f); ν_{RF}^H during heteronuclear decoupling = 100 kHz (c, d, g); ν_{RF}^H during FSLG = 100 kHz (g); τ_{CP} = 1 ms (c), 5 ms (d), 0.2 ms (g); τ_{RD} = 1 s (a, b), 1.5 s (c, d, g) and 6 s (e, f); NS = 14000 (a), 100 (b), 256 (c), 8 (d), 4 (e) and 32 (f); AT = 43 h (g).

^{11}B resonances are located at −148 ppm and −1.6 ppm, respectively, in agreement with earlier studies of BF_4^- anions.[18,37−43]

3.2.2. Characterization of the Cationic and Anionic Parts of the Supported [Pd(dppp)(dtc)]BF$_4$ Complex. Figure 4 shows spectra of the supported complex (sample PdBS15) taken under similar conditions as the corresponding results in Figure 3. The observed chemical shifts are listed in the last column of Table 2. Sample PdBS15 features similar resonances to those observed

Table 2. Chemical Shifts of Nuclei in [Pd(dppp)(dtc)]BF$_4$ and PdBS15 Measured by Liquid- and Solid-State NMR

	liquid-state	solid-state	
	$CDCl_3$	bulk	supported on silica
P1,5	10.6	13.6 8.0	11
C2,4	23.6	22.2 19.2	23
C3	18.6	18.0	18
C6	204.3	201.8	[a]
C8	44.2	43.2 42.8	44
C9	12.4	12.5	11
C*i*	128.0	[b]	130[c]
C*o*	132.8	[b]	130[c]
C*m*	129.1	[b]	130[c]
C*p*	131.7	[b]	130[c]
F	−	−148	−151 −155
B	−	−1.6	−2.8

[a] Not detected due to low S/N ratio. [b] Numerous resonances at: 140.0, 139.4, 134.6, 134.1, 133.6, 133.0, 132.1, 131.5, 130.8, 130.1, 129.3, 128.8, 128.2, 127.8, 127.1, 126.6, 126.1, 125.8, 125.4, 125.1, and 123.0 ppm. [c] Broad peak, not resolved.

in bulk [Pd(dppp)(dtc)]BF$_4$, which indicates that both ions of the palladium(II) complex retained their structure upon immobilization on the surface. The ^{13}C and ^{31}P resonances are notably broader in PdBS15 than in bulk [Pd(dppp)(dtc)]BF$_4$. In the case of ^{13}C spectra, the broadening is mainly due to the disordered nature of the silica surface. The resulting distributions of molecular conformations and local environments give rise to chemical shift dispersion which masks the spectral features resolved in the bulk complex. Similar disorder has been observed in the studies of tertiary phosphine complexes of platinum(II) covalently immobilized on silica support.[44] The ^{31}P line shape could not be fitted as a superposition of two (broadened) lines corresponding to sites P1 and P5 in the bulk (Figure 3d), implying that the structural distinction between P1 and P5 observed in bulk [Pd(dppp)(dtc)]BF$_4$ has been lost in PdBS15. Another possible explanation of spectral overlap involving molecular reorientation with a frequency in the kHz range (in the so-called intermediate motional regime) is less probable here. Indeed, the static ^{1}H line in PdBS15 had a full width at half-maximum (fwhm) of about 40 kHz, which is essentially the same as was found in three-dimensional bulk [Pd(dppp)(dtc)]BF$_4$ (∼50 kHz, spectra not shown), and typical of a fully rigid, strongly coupled system of ^{1}H nuclei. In other words, the anchored complexes are motionless on the relevant NMR time scale of <1 ms. The ^{1}H projections of ^{13}C{^{1}H} spectra in Figures 3g and 4e are shown in skyline mode, which is mainly responsible for the difference in the spectra. The ratios between aromatic and aliphatic protons in the sum projections of these spectra are the same within an error of 5%.

The dominant resonance in the ^{19}F spectrum of Figure 4c, representing the BF_4^- anion, is located at about −151 ppm (i.e., 3 ppm to higher shielding from bulk [Pd(dppp)(dtc)]BF$_4$). Also observed in this spectrum are a shoulder at −155 ppm and two additional peaks at −123 and −162 ppm. Valuable additional

(40) Frohn, H.-J.; Bardin, V. V. *Eur. J. Inorg. Chem.* **2006**, 3948–3953.
(41) Wrackmeyer, B. In *Annual Reports on NMR Spectroscopy*; Webb, G. A., Ed.; Academic Press: London, 1988; Vol *20*, pp 61−203.
(42) Noth, H.; Wrackmeyer, B. In *NMR Basic Principles and Progress*; Diehl, P., Fluck, E., Kosfeld, R., Eds.; Springer-Verlag: New York, 1978; Vol. 14.
(43) Lee, S.-I.; Saito, K.; Kanehashi, K.; Hatakeyama, M.; Mitani, S.; Yoon, S.-H.; Korai, Y.; Mochida, I. *Carbon* **2006**, *44*, 2578–2586.
(44) Bemi, L.; Clark, H. C.; Davies, J. A.; Fyfe, C. A.; Wasylishen, R. E. *J. Am. Chem. Soc.* **1982**, *104*, 438–445.

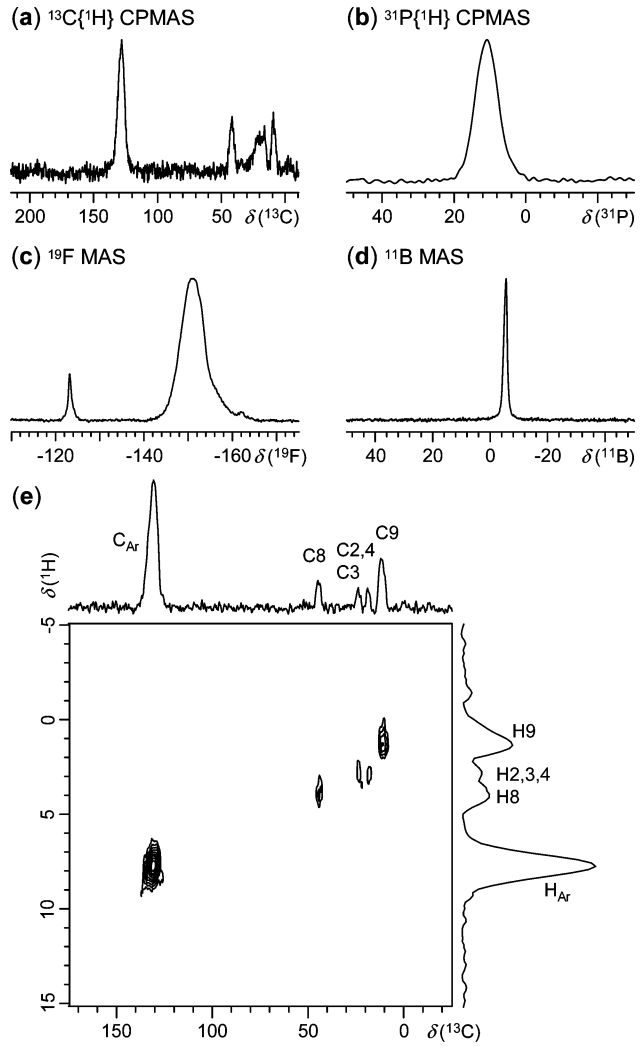

Figure 4. 1D (a−d) and 2D (e) NMR spectra of $[Pd(dppp)(dtc)]BF_4$ complex supported on silica (PdBS15). Experimental conditions: $B_0 = 14.1$ T (a, b, e) and 9.4 T (c, d); $\nu_R = 8$ kHz (a, b, e) and 40 kHz (c, d); ν_{RF}^H during heteronuclear decoupling = 100 kHz (a, b, e); ν_{RF}^H during FSLG = 100 kHz (e); $\tau_{CP} = 0.7$ ms (a), 5 ms (b) and 0.2 ms (e); $\tau_{RD} = 1.5$ s (a, b, e) and 2.5 s (c, d); NS = 16000 (a), 160 (b), 160 (c) and 320 (d); AT = 24 h (e).

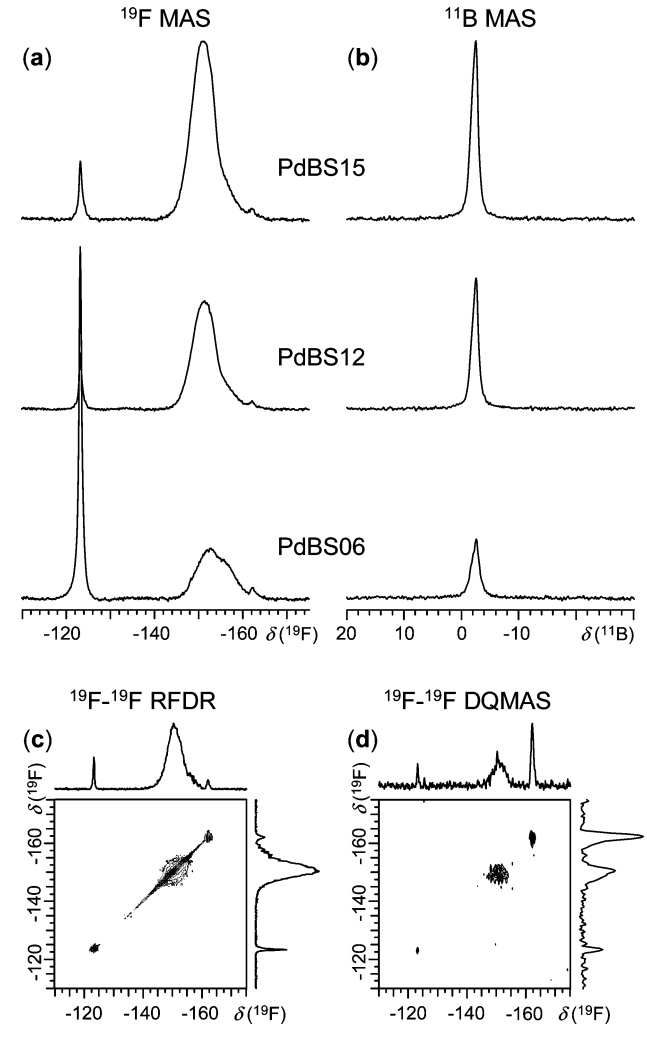

Figure 5. ^{19}F MAS (a), ^{11}B MAS (b), $^{19}F-^{19}F$ RFDR (c), and $^{19}F-^{19}F$ DQMAS (d) spectra of $[Pd(dppp)(dtc)]BF_4$ supported on SiO_2. Experimental conditions: $B_0 = 9.4$ T; $\nu_R = 40$ kHz; $\tau_{RD} = 2.5$ s (a, b, d) and 1.5 s (c); $\tau_{mix} = 20$ ms (c); $\tau_{DQ} = 200$ μs (d); NS = 160 (a) and 320 (b); AT = 15 h (c) and 2 h (d).

insights were offered by $^{19}F-^{19}F$ 2D RFDR and DQMAS NMR experiments (Figure 5c,d). The RFDR spectra showed that the broadening of the main ^{19}F resonance is mainly inhomogeneous under MAS at 40 kHz. When the mixing time τ_{mix} was set to 0 (spectrum not shown), the RFDR spectra of the supported complexes exhibited only diagonal peaks, with the homogeneous contribution to the line width (i.e., the width of the cross sections measured perpendicular to the diagonal) of only 180 Hz, or 0.5 ppm at 9.4 T. All ^{19}F nuclei exhibit strong dipolar coupling to other nuclei contributing to the same resonance, as evidenced by the diagonal cross-peaks in the DQMAS spectrum of Figure 5d. The fluorine species resonating at −123 and −162 ppm did not exchange magnetization with other fluorine atoms, even at $\tau_{mix} = 20$ ms (Figure 5c). The same spectrum also shows that the ^{19}F nuclei resonating at ∼−151 ppm exchange magnetization among themselves and with those observed at −155 ppm. The intensity of the resonance centered at ∼−155 ppm did not change with loading, which has important implications, as will be discussed later. Similarly, the peak at ∼−162 ppm retained its relative intensity of about 2−5%. However, the signal at ∼−151 ppm increased with increased loading adding to the total loading of 0.06 (PdPS06), 0.12 (PdBS12) and 0.15 (PdBS15) mmol/g. The BF_4^- anion appeared to be intact in all samples as evidenced by the presence of a single ^{11}B resonance at around −2.8 ppm in Figure 5b. The intensity of this resonance grew with increasing $[Pd(dppp)(dtc)]BF_4$ loading in the same manner as the sum of ^{19}F signals at −151 and −155 ppm.

On the basis of these data and the results of 2D $^{29}Si\{^{19}F\}$ HETCOR experiment (to be discussed in section 3.2.4), we assign the peak at −155 ppm to ^{19}F nuclei in BF_4^- anions interacting strongly with the silica surface, via hydrogen bonds with the surface hydroxyls. The resonances at −123 and −162 ppm most likely represent free F^- anion[37,45−48] (note that our NMR probe is Teflon-free) and 'bulk' BF_4^- species (note their high contribution to the DQMAS spectrum),[18,39−43] respectively. The origin of F^- anions remains unknown; however, the $^{19}F-^{19}F$ spectra showed that it is removed from the complex. It is

(45) Christe, K. O.; Wilson, W. W.; Wilson, R. D.; Bau, R.; Feng, J. A. *J. Am. Chem. Soc.* **1990**, *112*, 7619–7625.
(46) Christe, K. O.; Wilson, W. W. *J. Fluorine Chem.* **1990**, *47*, 117–120.
(47) Carmona, C.; Eaton, G.; Symons, M. C. R. *J. Chem. Soc., Chem. Commun.* **1987**, 873–874.
(48) Okabe, A.; Fukushima, T.; Ariga, K.; Niki, M.; Aida, T. *J. Am. Chem. Soc.* **2004**, *126*, 9013–9016.

Table 3. Concentration of [Pd(dppp)(dtc)]BF_4 Supported on Silica Determined by Quantitative Measurements of ^{11}B, ^{19}F, and ^{31}P Nuclei[a]

	final loading	surface coverage	
sample	[in mmol/g][b]	[in molecules per 100 nm^2][c]	[in %][d]
PdBS06	0.06 ± 0.01	7 ± 1	10 ± 2
PdBS12	0.12 ± 0.01	15 ± 1	20 ± 2
PdBS15	0.15 ± 0.01	18 ± 1	25 ± 2

[a] Quantitative DPMAS ^{29}Si spectra were also measured, which showed that the silica support has ~3.5 mmol of OH groups/g, or ~4.2/1 groups/nm^2 of the silica surface. [b] Average loading in mmol of [Pd(dppp)(dtc)]BF_4/g of silica obtained from ^{11}B, ^{19}F, and ^{31}P DPMAS data. [c] Number of [Pd(dppp)(dtc)]BF_4 molecules/100 nm^2 of silica. [d] Percent of silica surface that would be covered by [Pd(dppp)(dtc)]BF_4 complex assuming a [Pd(dppp)(dtc)]$^+$ size of 13 × 10.5 Å and monolayer surface coverage (no stacking).

possible that it was formed during defluorination reaction of BF_4^- anion with water (in the first step: $BF_4^- + H_2O \leftrightarrow BF_3(OH)^- + HF$)[49−51] or the silica surface.[18] The latter possibility is less likely due to lack of other three- or four-coordinated boron species (for example Si−O−BF_2 or Si−O−BF_3^-) in the ^{11}B spectra.[18,43,52,53] Furthermore, we were unable to demonstrate the existence of Si−O−B connectivities by $^{29}Si\{^{11}B\}$ NMR. We note that, in the static ^{19}F spectrum of PdBS15 (not shown), the resonances at −151 and −155 ppm form a single unresolved peak, with line width (13.6 kHz fwhm) similar to that of the crystalline [Pd(dppp)(dtc)]BF_4 complex (12.6 kHz fwhm). On the basis of the XRD data, the homonuclear dipolar coupling between neighboring ^{19}F nuclei in the rigid crystalline sample should be between 11 and 14 kHz. Thus, the BF_4^- anions also remain immobilized in PdBS15.

Finally, we compared the intensities of ^{11}B, ^{19}F and ^{31}P DPMAS spectra in samples PdBS06, PdBS12 and PdBS15 with those from a measured quantity of bulk [Pd(dppp)(dtc)]BF_4, as explained in the Experimental Section. The integration of ^{19}F, ^{11}B, and ^{31}P signals independently yielded very similar (within 10%) concentrations of the complex in each sample, as summarized in Table 3. In the next sections, we describe the mutual interactions between the cationic complex ligand, the BF_4^- anion, and the silica surface.

3.2.3. Interactions between the [Pd(dppp)(dtc)]$^+$ Cation and BF_4^- Anion. The proximity between the BF_4^- anions and the organic ligands in the cation was probed by double resonance NMR experiments involving nuclei from both parts of the complex, that is, ^{11}B or ^{19}F in BF_4^- and ^1H,^{13}C or ^{31}P of ligands in the cationic complex. Specifically, 1D $^{13}C\{^{19}F\}$ CPMAS, as well as 2D $^{11}B\{^1H\}$, $^{31}P\{^{19}F\}$ and $^{19}F\{^1H\}$ HETCOR spectra were acquired for bulk [Pd(dppp)(dtc)]BF_4 and sample PdBS15 (Figures 6 and 7). Internuclear correlations were generated in all these experiments, indicating close spatial proximity (within a few angstroms) between the studied nuclei. In bulk [Pd(dppp)(dtc)]BF_4, the ^{31}P resonances at 8 and 13.6 ppm in Figure 6a are correlated with the ^{19}F resonance at around −148 ppm, which we earlier assigned to BF_4^- anions. The ^{11}B nuclei were polarized by protons in both aliphatic and aromatic parts of the spectrum (Figure 6b). Note that the ^{31}P dimension in Figure 6a has lower resolution than the $^{31}P\{^1H\}$ CPMAS spectrum in Figure 3d, which is due to lack of ^1H decoupling. Also, ^1H resolution in the spectrum of Figure 6b is lower than in the 2D $^{13}C\{^1H\}$ HETCOR spectrum of Figure 3g, because only the latter was acquired using the FSLG ^1H homonuclear decoupling. The 2D $^{19}F\{^1H\}$ HETCOR and 1D $^{13}C\{^{19}F\}$ spectra of bulk [Pd(dppp)(dtc)]BF_4 are shown in Figure 7. Again, the main ^{19}F signal at −148 ppm is correlated with ^1H signals in the aliphatic and aromatic regions, even for contact times as short as 0.08 ms. Similarly, the $^{13}C\{^{19}F\}$ spectrum in Figure 7b shows strong correlations with the phenyl rings as well as carbons C8 and C9.

The same correlations were observed in all spectra of PdBS15, which suggests that the relative positions of the cationic and anionic components of the complex have not changed appreciably in the silica supported environment. We also verified that the relative efficiencies with which ^{13}C and ^{31}P nuclei were polarized by the nuclei in the cationic (^1H) and ionic (^{19}F) parts of the complex were comparable in both samples.

The exact internuclear distances in bulk [Pd(dppp)(dtc)]BF_4 and PdBS15 are difficult to measure by NMR because of the large number of interacting spins and structural heterogeneity. However, even semiquantitative evaluation of the NMR data can lead to useful insights. For example, the efficiency of CP within an isolated pair of spin-1/2 nuclei should reach its maximum at $(\tau_{CP})^{opt} = 1.7/D$, where D is the dipolar coupling constant and the assumption is made that the experiment uses the first sideband of the Hartmann−Hahn matching curve.[54] In the $^{31}P\{^{19}F\}$ CPMAS measurements on bulk [Pd(dppp)(dtc)]BF_4 and PdBS15, we found $(\tau_{CP})^{opt} \approx 5$ ms (see caption to Figure 7), which corresponds to $D = 340$ Hz and a $^{31}P-^{19}F$ distance of ~5.2 Å. Bearing in mind that (i) the samples studied by NMR did not contain chloroform, (ii) our estimate of $(\tau_{CP})^{opt}$ did not include multispin interactions, and (iii) we ignored the presence of $T_{1\rho}$ relaxation (which would reduce $(\tau_{CP})^{opt}$), we find this result to be in good agreement with the shortest $^{31}P-^{19}F$ distance of ~6.4 Å measured by XRD in bulk [Pd(dppp)(dtc)]BF_4.[32]

In this context, it is interesting to note that the correlations between ^1H or ^{13}C in aliphatic parts of the cations and ^{19}F or ^{11}B nuclei in the anions in bulk [Pd(dppp)(dtc)]BF_4 and PdBS15 are also stronger than would be expected from the crystalline structure shown in Figure 2. In the case of $^{13}C\{^{19}F\}$ CPMAS, the polarization of carbons C8 and C9 using $\tau_{CP} = 2$ ms is almost as efficient as the polarization of the phenyl rings. This would not be observed if the average distance between ^{19}F and these nuclei was on the order of 7 Å as in the [Pd(dppp)(dtc)]$BF_4 \cdot 2CHCl_3$ crystal studied by XRD.[32] The resonances representing aliphatic protons are surprisingly intense in $^{11}B\{^1H\}$ and $^{19}F\{^1H\}$ HETCOR spectra in Figures 6b,d and 7a. Again, these findings are attributed to a lack of chloroform in the structure of bulk and supported [Pd(dppp)(dtc)]BF_4, and the resulting compression of its structure.

3.2.4. Interaction between the BF_4^- Anion and the Silica Surface. This part of the study involved a challenging 2D $^{29}Si\{^{19}F\}$ HETCOR experiment, which was enabled by the use of CPMG refocusing during ^{29}Si detection (Figure 8a).[27,28] Also shown, in Figure 8b, is the ^{19}F projection of this spectrum in comparison with the ^{19}F DPMAS and $^{19}F\{^{11}B\}$ CPMAS spectra of the same sample and, in Figure 8c, the ^{29}Si projection superimposed with the corresponding $^{29}Si\{^1H\}$ CPMAS spectrum. The 2D spectrum shows a dominant correlation between

(49) Kuhlmann, K.; Grant, D. M. *J. Phys. Chem.* **1964**, *68*, 3208–3213.
(50) Wamser, C. A. *J. Am. Chem. Soc.* **1948**, *70*, 1209–1215.
(51) Wamser, C. A. *J. Am. Chem. Soc.* **1951**, *73*, 409–416.
(52) Fild, C.; Shantz, D. F.; Lobo, R. F.; Koller, H. *Phys. Chem. Chem. Phys.* **2000**, *2*, 3091–3098.
(53) Koller, H.; Fild, C.; Lobo, R. F. *Microporous Mesoporous Mater.* **2005**, *79*, 215–224.
(54) Amoureux, J. P.; Pruski, M. *Mol. Phys.* **2002**, *100*, 1595–1613.

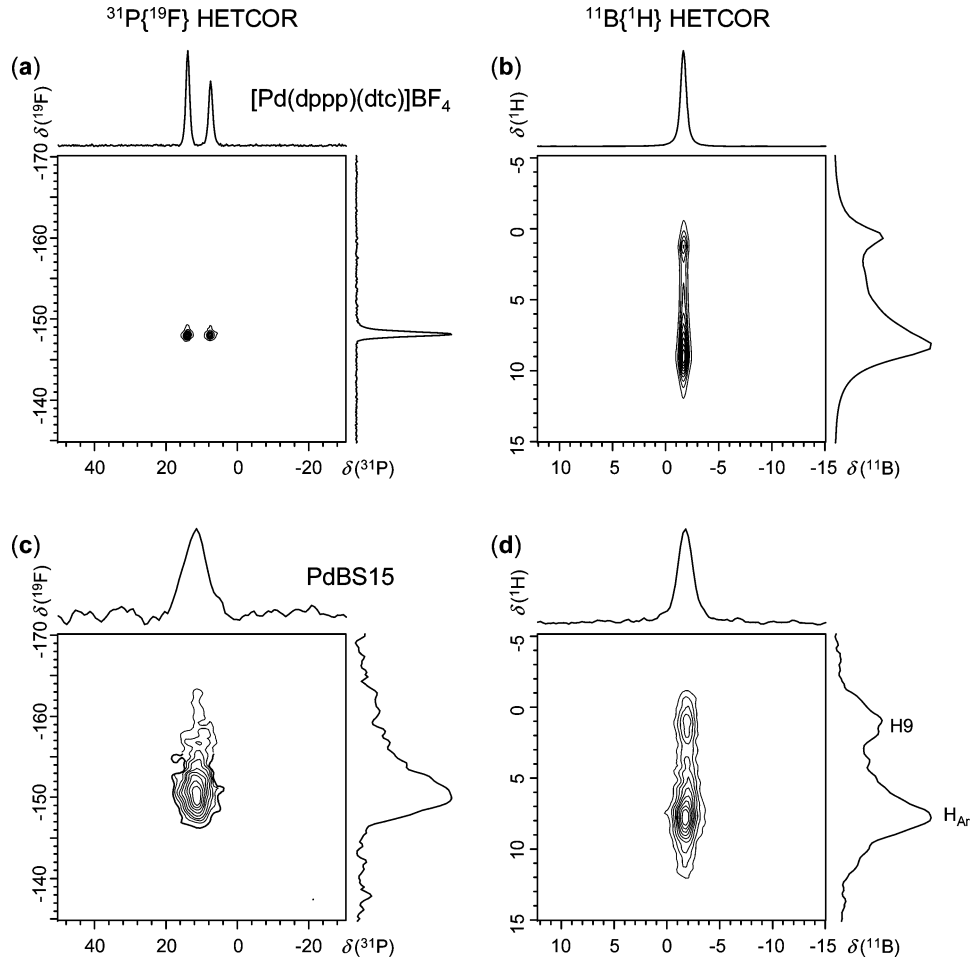

Figure 6. 2D $^{31}P\{^{19}F\}$ (a and c) and $^{11}B\{^{1}H\}$ (b and d) HETCOR spectra of samples $[Pd(dppp)(dtc)]BF_4$ (a and b) and PdBS15 (c and d). Experimental conditions: $B_0 = 9.4$ T; $\nu_R = 40$ kHz; ν_{RF}^H during heteronuclear decoupling = 11 kHz (a and c); $\tau_{CP} = 5$ ms (a and c) and 0.7 ms (b and d); $\tau_{RD} = 2.5$ s (a and b) and 0.7 s (c and d); AT = 5 h (a), 6.5 h (b), 19 h (c) and 4 h (d).

the silica sites Q^4 in the support and those ^{19}F nuclei in the BF_4^- anion that contributed to the shoulder around −155 ppm in the ^{19}F DPMAS spectrum. A weaker cross-peak, comprising about 20% of the observed ^{29}Si signal, represents the correlation with silicon sites Q^3. In the $^{29}Si\{^{1}H\}$ CPMAS spectrum of Figure 8c, sites Q^3 account for more than 60% of the observed intensity. The study of $^{19}F \rightarrow {}^{29}Si$ CP dynamics (not shown) indicated that the polarization of Q^4 occurred at a faster rate than Q^3, which demonstrates that the distance between fluorine and Q^4 is (on average) closer.

Accordingly, we assign the peak at −155 ppm to fluorine atoms that are hydrogen bonded to the surface hydroxyl groups, but are located closer to sites Q^4. As already mentioned in section 3.2.2, the intensity of this resonance was independent of the $[Pd(dppp)(dtc)]BF_4$ loading, which implies the existence of two separate groups of BF_4^- anions. A fixed population of species, which emerges at low $[Pd(dppp)(dtc)]BF_4$ loading, is immobilized directly on silica via one or more hydrogen bonds. Only the hydrogen-bonded fluorine atoms in these BF_4^- anions resonate at −155 ppm, while those which are not hydrogen-bonded contribute to the peak at −151 ppm. A second population of BF_4^- species, which increases with increased $[Pd(dppp)(dtc)]BF_4$ loading and also contributes to the peak at −151 ppm, is not immobilized directly on the silica surface. The deconvolution of the ^{19}F MAS spectrum revealed that the intensity ratio between peaks at −155 and at −151 ppm is about 1:2 in PdBS06 and 1:6.5 in PdBS15. Although the exact number of hydrogen bonds formed by a single BF_4^- anion is unknown, the surface-bound BF_4^- anions can form between one and three hydrogen bonds with the neighboring hydroxyl groups. Indeed, by comparing the measured surface concentration of the OH groups with the size of the $[Pd(dppp)(dtc)]BF_4$ complex (see the footnotes to Table 3), it is evident that on average each complex could interact with 5−6 surface hydroxyls. By assuming that statistically two such bonds exist per BF_4^- anion and using the results from Table 3, the concentration of surface bound $[Pd(dppp)(dtc)]BF_4$ complexes is estimated at 0.04 mmol/g in all samples. Consequently, a considerable fraction of the $[Pd(dppp)(dtc)]BF_4$ complexes (on the order of 1/3 in PdBS06 and 3/4 in PdBS15) does not reside directly on the surface. We will discuss this further in the Conclusion.

3.2.5. Interaction between the Cationic $[Pd(dppp)(dtc)]^+$ Complex and the Silica Surface. The location of the complex cations which reside directly on the silica surface was probed by $^{29}Si\{^{1}H\}$ HETCOR-CPMG NMR.[27,28] Two samples with the lowest and highest $[Pd(dppp)(dtc)]BF_4$ concentrations (PdBS06 and PdBS15) were examined. Since the spectra were very similar, only one corresponding to PdBS15 is shown in Figure 9. In this spectrum, strong correlations were detected between all silicon sites (Q^3 and Q^4) and proton resonances representing phosphine and dtc regions of the cationic complex. This result indicates that those cationic complexes which do interact directly with the surface reside in the prone position (parallel to the silica surface). Again, the ^{1}H projections shown in Figures 9

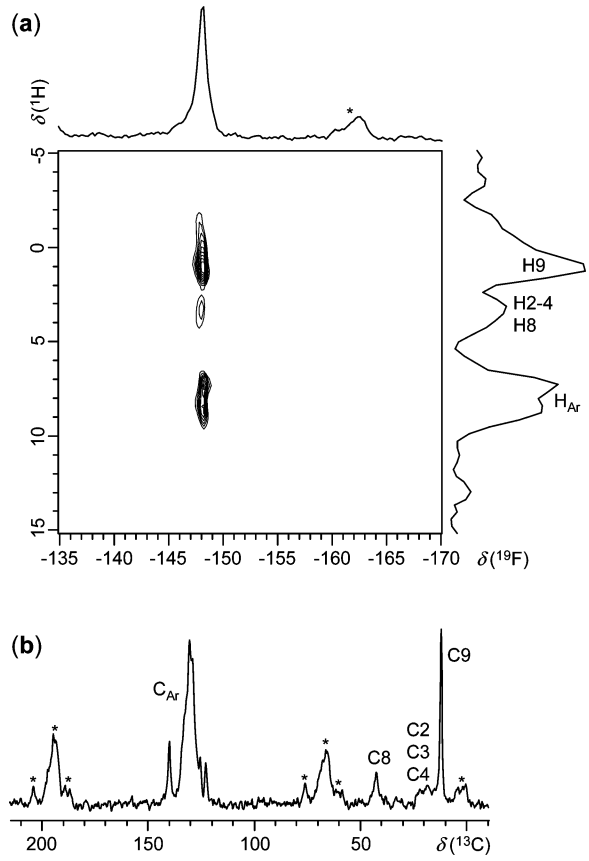

Figure 7. $^{19}F\{^1H\}$ HETCOR (a) and $^{13}C\{^{19}F\}$ CPMAS (b) spectra of bulk [Pd(dppp)(dtc)]BF_4. Experimental conditions: $B_0 = 11.7$ T; $\nu_R = 13.7$ kHz (a) and 8 kHz (b); $\tau_{CP} = 0.2$ ms (a) and 2 ms (b); ν_{RF}^H during PMLG = 89 kHz (a), ν_{RF}^H during heteronuclear decoupling = 50 kHz (a and b); ν_{RF}^F during heteronuclear decoupling = 40 kHz (b); $\tau_{RD} = 1.5$ s (a) and 2 s (b); scaling factor = 0.56; AT = 1 h (a); NS = 40302 (b). Asterisks in the spectra denote the spinning sidebands.

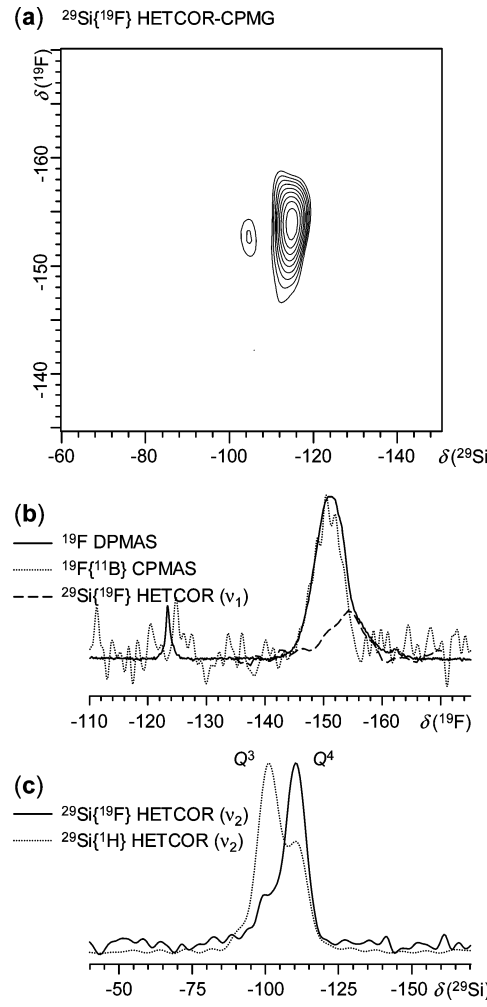

Figure 8. 2D $^{29}Si\{^{19}F\}$ HETCOR-CPMG spectrum of sample PdBS15 (a). Experimental conditions: $B_0 = 9.4$ T; $\nu_R = 40$ kHz; $\tau_{CP} = 15$ ms; $\tau_{CPMG} = 4$ ms; $N_{CPMG} = 200$; $\tau_{RD} = 6$ s; AT = 48 h. In panel (b), ^{19}F projection of this spectrum (dashed line) is compared with ^{19}F DPMAS spectrum of Figure 4c (solid line) and 1D $^{19}F\{^{11}B\}$ CPMAS spectrum (dotted line) acquired under similar conditions with $\tau_{CP} = 20$ ms, $\tau_{RD} = 6$ s and NS = 3000. Panel (c) compares the ^{29}Si projections of panel (a) (solid line) and Figure 9 (dotted line).

and 6d are notably different. The intensity around 5 ppm may be due to SiOH-$(H_2O)_n$ species, which are likely to be present on silica surface in spite of deuteration.[15] We finally note that integrated intensities of $^{29}Si\{^1H\}$ spectra of PdBS06 and PdBS15, normalized with respect to the weight of silica, were the same within the experimental error of 10%. This finding is consistent with the constant concentration of surface-bound BF_4^- anions in these samples.

4. Conclusion

The XRD and NMR studies described above provide substantial information about the structure of [Pd(dppp)(dtc)]BF_4 and about interactions of the Pd(II) complex cation and the BF_4^- anion with the surface of the silica support. The XRD study of [Pd(dppp)(dtc)]BF_4 showed a square planar arrangement of two P and two S atoms around the Pd. Solid-state NMR data showed that the structures of cationic and anionic parts are essentially the same whether [Pd(dppp)(dtc)]BF_4 is supported or unsupported; however, the inequivalence of some of the sites in the crystalline structure is lost upon anchoring [Pd(dppp)(dtc)]BF_4 on silica. In addition, loss of resolution has been observed in ^{13}C, ^{19}F, and ^{31}P spectra, which is attributable to the heterogeneity of local environments on the silica surface. The overall [Pd(dppp)(dtc)]BF_4 loading has been determined by quantitative measurements of ^{11}B, ^{19}F, and ^{31}P intensities. The proximities between $[Pd(dppp)(dtc)]^+$ cation, the BF_4^- anion and the silica surface have been clearly established by the applied HETCOR NMR methods and found to be similar to those in the bulk sample.

Finally, we summarize the key findings that point us toward understanding the structure of [Pd(dppp)(dtc)]BF_4 immobilized on silica. (1) 1D $^{13}C\{^{19}F\}$, as well as 2D $^{11}B\{^1H\}$, $^{31}P\{^{19}F\}$, and $^{19}F\{^1H\}$ spectra, demonstrated that the relative locations of the cationic and anionic components in the supported complex remain very similar to those in the bulk. (2) There exists a population of BF_4^- anions that are immobilized in the vicinity of silicon sites Q^4. The concentration of these sites corresponds to BF_4^- loading of about 0.04 mmol/g, regardless of the overall loading of [Pd(dppp)(dtc)]BF_4 in the sample. (3) Strong correlations have been detected between the phosphine and amine regions of the cationic complex and silicon sites Q^3 and Q^4, demonstrating the horizontal position of $[Pd(dppp)(dtc)]^+$ on the silica surface. Again, the intensity of the observed $^1H-^{29}Si$ correlations is independent of the overall [Pd(dppp)(dtc)]BF_4 concentration, suggesting that only some of the complexes are within a few angstrom from the silica surface. (4) No molecular

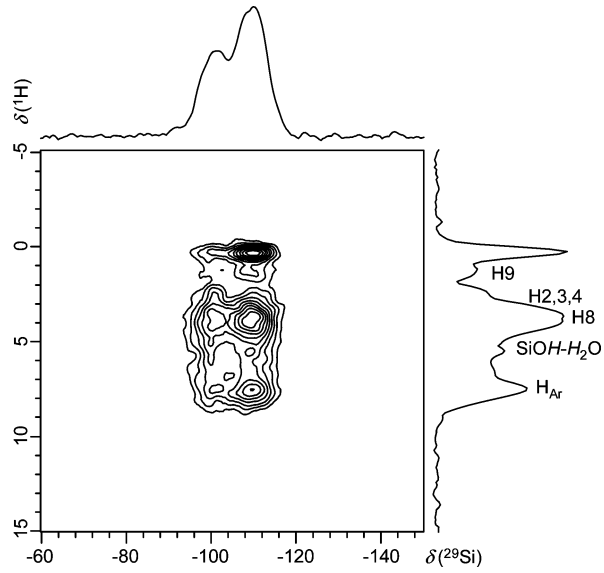

Figure 9. 2D $^{29}Si\{^{1}H\}$ HETCOR spectrum of sample PdBS15. Experimental conditions: $B_0 = 9.4$ T; $\nu_R = 40$ kHz; $\tau_{CP} = 8$ ms; $\tau_{CPMG} = 4$ ms; $N_{CPMG} = 200$; $\tau_{RD} = 0.2$ s; AT = 16 h.

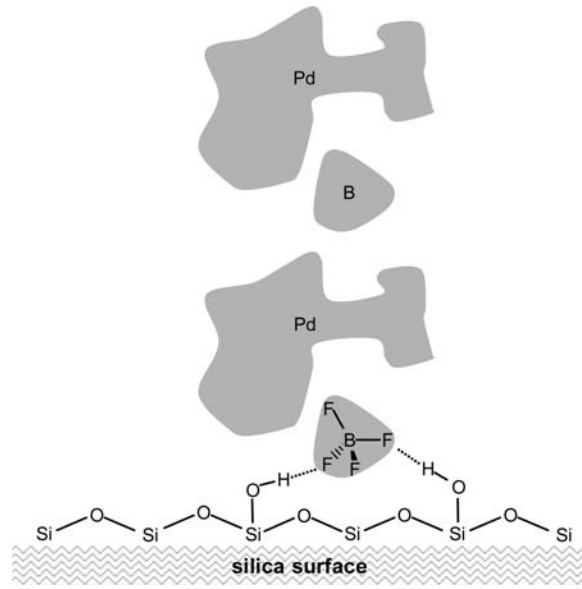

Figure 10. Anchoring of $[Pd(dppp)(dtc)]BF_4$ on the silica surface.

mobility on the time scale of <1 ms was detected in the static ^{1}H and ^{19}F NMR spectra.

On the basis of these data, it seems evident that, at $[Pd(dppp)(dtc)]BF_4$ loadings of ≤0.04 mmol/g, the BF_4^- anions are immobilized directly on the surface near the Q^4 sites. Most likely, the surface-bound BF_4^- anions form multiple hydrogen bonds with the neighboring silica hydroxyl groups. The $[Pd(dppp)(dtc)]^+$ cations are anchored to these anions in a similar configuration as in the bulk material, assuming a horizontal position on the surface. When the overall loading of $[Pd(dppp)(dtc)]BF_4$ increases, the complexes stack on top of each other, as depicted in Figure 10. It is interesting to note that, with ratios of directly adsorbed to stacked complexes being roughly 2:1 in sample PdBS06 and 1:3 in sample PdBS15, it follows from the data in Table 3 that directly adsorbed molecules take up less than 10% of the silica surface.

This model agrees with the findings of our IR studies of $(\eta^5\text{-}C_5H_5)Ru(CO)_2(BF_4)$ adsorbed on SBA-15,[11] but differs from those proposed earlier for other BF_4^- salts.[17,18] In the study of $[Rh_2(NCCH_3)_{10}](BF_4)_4$ on MCM-41,[17] the existence of Si−O−Rh bonds was postulated based primarily on the observed reduction of resonances representing Q^2 and Q^3 silicon environments relative to Q^4 in the ^{29}Si CPMAS spectra upon grafting the Rh complex. Our measurements showed that similar variations in the CPMAS intensities could be attributed to more efficient polarization of Q^4 sites after adsorption of the complex. The ^{11}B spectra observed in silica supported $[(\eta^5\text{-}C_5H_5)Fe(CO)_2(THF)]BF_4$ included a sharp ^{11}B peak at −3.5 ppm attributed to $Si-O-BF_3^-$ species on the silica surface.[18] Since the ^{11}B spectrum also included a broad intense peak characteristic of trivalent species, it was postulated that $Si-O-BF_3^-$ converted to $Si-O-BF_2$ with the lost fluorine forming hydrofluoric acid and possibly fluorinating the silica surface. Again, we have not observed trivalent boron in any of our samples and were unable to establish Si−O−B or Si−F connectivities.

The stacking of BF_4^- salts of metal complexes on silica, which is reported here for the first time, has important consequences for catalysis by such salts. It means that increasing the loading of a catalytic complex-BF_4 salt ($Cat^+BF_4^-$) on silica would not increase the amount of accessible catalyst, even though only a small fraction of the silica surface is covered by the $Cat^+BF_4^-$. This stacking of complexes suggests that $Cat^+BF_4^-$ adsorbs at only specific sites on the silica. Additional $Cat^+BF_4^-$ then finds the stacked arrangement (Figure 10) more energetically favorable. Of course, the average activity of each $Cat^+BF_4^-$ unit at high loading would be lower than that at low loading, which would be reflected in lower TON and TOF values. The tendency of a supported $Cat^+BF_4^-$ catalyst to form stacks or to spread out on the silica surface undoubtedly depends upon the thermodynamics of these two processes, which may vary with the nature of the cation Cat^+.

Acknowledgment. This research was supported at the Ames Laboratory by the U.S. Department of Energy, Office of Basic Energy Sciences, under Contract No. DE-AC02-07CH11358.

Supporting Information Available: The ORTEP structure of $[Pd(dppp)(dtc)]BF_4 \cdot 2CHCl_3$ complex (Figure S1), all crystallographic data (Tables S1−S6), and CIF data file for $[Pd(dppp)(dtc)]BF_4 \cdot 2CHCl_3$ complex. This material is available free of charge via the Internet at http://pubs.acs.org.

JA902982U